Analysis of diagnostic climate model cloud parameterisations using large-eddy simulations

J. Rosch[a], T. Heus[b], M. Brueck[a], M. Salzmann[a], J. Mülmenstädt[a], L. Schlemmer[c] and J. Quaas[a]*

[a]*Universität Leipzig, Institute for Meteorology, Stephanstr. 3, D-04103 Leipzig*

[b]*Department of Physics, Cleveland State University, 2121 Euclid Ave. , Cleveland, OH 44115*

[c]*Max-Planck-Institut für Meteorologie, Bundesstr. 53, D-20146 Hamburg*

*Correspondence to: johannes.quaas@uni-leipzig.de

Current climate models often predict fractional cloud cover on the basis of a diagnostic probability density function (PDF) describing the subgrid-scale variability of the total water specific humidity, q_t, favouring schemes with limited complexity. Standard shapes are uniform or triangular PDFs the width of which is assumed to scale with the grid-box mean q_t or the grid-box mean saturation specific humidity, q_s. In this study, the q_t variability is analysed from large-eddy simulations for two stratocumulus, two shallow cumulus, and one deep convective cases. We find that in most cases, triangles are a better approximation to the simulated PDFs than uniform distributions. In two of the 24 slices examined, the actual distributions were so strongly skewed that the simple symmetric shapes could not capture the PDF at all. The distribution width for either shape scales acceptably well with both the mean value of q_t and q_s, the former being a slightly better choice. The q_t variance is underestimated by the fitted PDFs, but overestimated by the existing parameterisations. While the cloud fraction is in general relatively well diagnosed from fitted or parameterised uniform or triangular PDFs, it fails to capture cases with small partial cloudiness, and in 10 – 30% of the cases misdiagnoses clouds in clear skies or vice-versa. The results suggest choosing a parameterisation with a triangular shape, where the distribution width would scale with the grid-box mean q_t using a scaling factor of 0.076. This, however, is subject to the caveat that the reference simulations examined here were partly for rather small domains and driven by idealised boundary conditions.

Key Words: Cloud parameterisation, climate modelling, large-eddy simulations, total water specific humidity, probability density function

Received 0000

1. Introduction

Since cloud processes occur at scales not resolved by current general circulation models (GCMs), they have to be parameterised by statistical descriptions. The fundamental parameterisation is the prediction or diagnosis of fractional cloud cover. If fractional cloud cover (i.e. the possibility for a cloud fraction, $0 < f < 1$) is parameterised, this implies knowledge about the statistical distribution of the subgrid-scale variability of relative humidity. It is usually assumed that variability in relative humidity mostly stems from variability in specific humidity, with saturation specific humidity, or equivalently, temperature, taken as homogeneous across each model grid-box. The subgrid-scale variability is then described in terms of the total-water specific humidity, q_t, which is conserved for phase changes. The most basic description of subgrid-scale variability of q_t is a diagnostic probability density function (PDF).

Two of the cloud schemes commonly used in current GCMs assume a rectangular (uniform, top-hat) shape of the PDF (Sundqvist *et al.* 1989; Le Treut and Li 1991) and a triangular shape (Smith 1990), respectively. While newer developments allow for flexible use of these simple schemes (Watanabe *et al.* 2009), the original formulations are still widely used (e.g., Stevens *et al.* 2013). Both the rectangular and the triangular PDF are considered symmetric in these schemes, and their mean value is the predicted grid-box mean value of q_t. The flexible parameter is the distribution width. Smith (1990) parameterises the half-width of the assumed triangular distribution as

$$\Delta q_t = \gamma q_s \tag{1}$$

with $\gamma = 0.075$ in their lowest two model layers (up to layer σ = 0.9, with sigma the pressure fraction of surface pressure, or about 900 hPa) and $\gamma = 0.15$ in the free troposphere*. Sundqvist *et al.* (1989) uses a half-width of the assumed rectangular distribution that also scales with q_s, as in Eq. 1, but with $\gamma = 0.1$ near the surface and $\gamma = 0.3$ in the free troposphere (Stevens *et al.* 2013). In contrast, Le Treut and Li (1991) parameterise the half-width of the rectangular PDF scaling with the mean total-water specific humidity, as

$$\Delta q_t = \gamma \bar{q}_t \tag{2}$$

with $\gamma = 0.2$ throughout the atmosphere in their original implementation. The main points of the three parameterisations analysed are summarised in Table 1.

Total-water subgrid-scale variability has been investigated elsewhere by analysing large-eddy simulations (e.g., Tompkins 2002; Perraud *et al.* 2011; Naumann *et al.* 2013) and observations (e.g., Weber *et al.* 2011; Boutle *et al.* 2013). These studies demonstrate that at scales of current GCMs, the shapes of PDFs are often intricate, including bi-modal distributions. Comprehensive PDF shapes such as double-Gaussian distributions fit the simulated or observed distributions better than simpler shapes (Larson *et al.* 2002; Bogenschutz *et al.* 2010; Perraud *et al.* 2011). However, sophisticated prognostic statistics of the total-water subgrid-scale variability imply complex parameterisations with many degrees of freedom that are difficult to digest for coarsely resolved global climate models and hard to constrain from observations (e.g., Quaas 2012). In consequence of this, for example, the ECHAM6 model (Stevens *et al.* 2013) returned to the Sundqvist *et al.* (1989) cloud scheme due to difficulties with the prognostic cloud scheme by Tompkins (2002) that was used in ECHAM5 (Roeckner *et al.* 2003).

The aim of the present study is thus to examine simple, diagnostic cloud parametersations. Specifically, we ask the following two questions:

1. Which of a triangular or a rectangular PDF better describes the subgrid-scale variability of the total-water specific humidity?
2. Which proposition to parameterise the distribution width is best?

These two questions are addressed by analysing the output of available large-eddy simulations (LES) for various cloud regimes.

2. Methods

The large-eddy simulations analysed here have been performed with the UCLA LES model (Stevens *et al.* 2005). We use two cases of stratocumulus over ocean (cases S11 and S12 of the

*The original formuation further takes the impact of phase changes on q_s into account, by their factor a_L which is set to 1 here for simplicity.

Table 1. Summary of the parameterisations analysed: Shape and half-width Δq_t, of the q_t PDF, scaling values in the boundary layer and in the free troposphere, and references.

	Shape	Δq_t	γ boundary layer	γ free troposphere	Reference
1.	Triangular	$\Delta q_t = \gamma q_s$	0.100	0.30	Smith (1990)
2.	Rectangular	$\Delta q_t = \gamma q_s$	0.075	0.15	Sundqvist *et al.* (1989)
3.	Rectangular	$\Delta q_t = \gamma \bar{q}_t$	0.200	0.20	Le Treut and Li (1991)

Table 2. Set-up and basic results of the large-eddy simulations analysed.

Case	Cloud type	Domain	Resolution	Cloud base	Cloud top	Duration	Reference
S12	Stratocumulus	2.4×2.4 km^2	25 m	400 m	700 m	10 d	Blossey *et al.* (2013)
S11	Stratocumulus over cumulus	4.8×4.8 km^2	50 m	650 m	1500 m	10 d	Blossey *et al.* (2013)
S6	Trade cumulus	9.6×9.6 km^2	100 m	500 m	2800 m	10 d	Blossey *et al.* (2013)
RICO	Trade cumulus	102×102 km^2	25 m	600 m	1500 m	35 h	Seifert and Heus (2013)
DEEP_cu	Deep convection case initial stage (cumulus)	256×256 km^2	250 m	600 m	2500 m	24 h	Schlemmer and Hohenegger (2014
DEEP_cb	Deep convection case developed stage				10 km		

CGILS project, Zhang *et al.* 2013; Blossey *et al.* 2013), two cases of marine shallow cumulus (case S6 of CGILS and the RICO case of VanZanten *et al.* 2011), and the deep convective case of Schlemmer and Hohenegger (2014, their WET case), which in the initial phase also corresponds to a cumulus case and later on, to a deep convective case; these two phases are analysed separately. The simulations are summarised in Table 2. As discussed by Schlemmer and Hohenegger (2014), the - for an LES - rather coarse resolution of 250 m is sufficient in this case and well within the inertial subrange (see also Petch *et al.* 2002; Bryan *et al.* 2003). The PDF of total-water specific humidity is meant to sample spatial variability in the horizontal dimension at each GCM model level (of $\mathcal{O}$(200 m) depth) within each time step (of $\mathcal{O}$(10 min) length). From the LES simulations, we thus use the full model domain to analyse the horizontal variability, at selected individual levels and selected time-steps after model spin-up. Levels were selected subjectively to correspond to the below-cloud-, lower-cloud-, upper-cloud- and above-cloud layers with the below- and above-cloud layers well apart from the upper or lower model boundary. The time-steps were chosen to be in the (quasi-)equilibrium cloud situation.

At each selected level and time-step, the mean value of q_t is computed and taken as the mean of the PDF. The width of rectangular and triangular PDFs, respectively, is then computed by a maximum-overlap fit to the LES-simulated PDF (choosing a least-squares fit vs. the maximum-overlap fit does not impact the conclusions). For diagnostic purposes, we also compute the domain-average temperature and from it the saturation specific humidity. The cloud fraction is computed from LES output, as well as from the LES-simulated PDF as the fraction of the PDF exceeding q_s computed from the grid-box mean temperature, and equally so for the two fitted PDFs.

3. Results and discussion

The analysis is performed in three steps. Firstly, we assess to which extent in general a symmetric PDF of either rectangular or triangular shape may fit the LES-simulated distributions of q_t. Secondly, given the perfectly-fitted simple-shaped PDFs, we evaluate how well their width might be parameterised using grid-box mean information. Finally, the cloud cover as diagnosed from the parameterisations is evaluated against the actually simulated cloud cover.

3.1. Fits of rectangular and triangular PDFs

The PDFs of q_t from the selected situations, as well as the fitted uniform and triangular distributions, are shown in Fig. 1. There are several issues found when fitting the simple diagnostic PDFs.

- The LES-simulated q_t PDFs are often not symmetric. Rather, in the below-cloud layer in five of the six cases, the PDF is negatively skewed, and it is positively skewed in five cases in the lower part of the cloud, and also in four cases in the upper cloud part. In consequence, the use of the

Figure 1. PDFs of q_t as simulated by the LES (black plain), fitted rectangular (red, dashed) and triangular (blue, dotted) PDFs. The vertical black line indicates q_s diagnosed from the domain-mean temperature. Columns from left to right are the S11, S12, S6, RICO, DEEP_cu and DEEP_cb cases. Rows are for each case selected layers, from top to bottom: above cloud top, in upper part of cloud, in lower part of the cloud, below cloud base. For each case, a time-step representative of the developed, where applicable: equilibrium, cloud regime is selected. The x-axis does not always span the entire PDF range from minimum to maximum value, especially not in the heavily skewed cases such as the RICO above-cloud layer case.

Figure 2. Scatterplot of distribution width for (a,b) rectangular and (c,d) triangular shapes as a function of (a,c) q_s and (b,d) $\bar{q}_t$ for the cases shown in Fig. 1. Red: S12, blue: S11, green: S6, purple: RICO, orange: DEEP_cu, yellow: DEEP_cb. Triangles up: above-cloud level, diamonds: upper cloud level, squares: lower cloud level, triangles down: below-cloud level. The red line indicates the regression fit forced through zero, and the pink shading $\pm$ one standard deviation of the fit. The grey-shaded area in (a) encompasses the near-surface and free-troposphere values of the Sundqvist *et al.* (1989) parameterisation, the grey line in (b) is the Le Treut and Li (1991) parameterisation, and the grey-shaded area in (c), the range as parameterised by Smith (1990).

Figure 3. Scatterplot of the standard deviation of q_t as computed from the LES data vs. (left) the standard deviation as computed by the fitted uniform and (right) the fitted triangular PDF. Cases are by colour and layers by symbol as in Fig. 2. Statistics are given in the upper left of each panel, i.e., the correlation coefficient r^2, the slope of the linear regression line, β, the mean bias standard deviation of the fit minus of the LES data, and corresponding root-mean-square deviation.

grid-box mean q_t as mean of the PDF is not often a good choice, it sometimes completely fails such as in the above-cloud layer of the RICO case, where some clouds penetrate into the free troposphere rendering the PDF very skewed.

- The PDFs show a distinct mode, rather than being very broad, so that the triangular shape tends to be a better fit.
- The saturation specific humidity computed from the grid-box mean temperature is in general within the PDF for the in-cloud cases, and outside the range for the below- or above-cloud layers (with two exceptions at the below-cloud layer in the S12 and RICO cases[†]). However, the fitted PDFs are often not wide enough to encompass q_s for the in-cloud cases.

These deficiencies certainly are to be expected: A PDF assuming a simple shape as rectangular or triangular, for which symmetry is assumed and the mean value is given by the model, necessarily cannot perfectly fit the actual PDF in each case. In the remainder, keeping in mind the documented shortcomings, we will assume the fitted rectangular and triangular PDFs represent acceptably well the actual PDFs, and assess the parameterised width of the diagnosed PDFs.

3.2. Parameterisation of the width of the PDFs

From the fitted rectangular and triangular PDFs as shown in Fig. 1, the width is diagnosed. In the parameterisations discussed, the width of the PDF, expressed as half-width Δq_t, is related to the grid-box mean total-water specific humidity, $\bar{q}_t$ (Le Treut and Li 1991), or the saturation specific humidity diagnosed from the grid-box mean temperature, q_s (Sundqvist *et al.* 1989; Smith 1990), respectively. Fig. 2 shows for both rectangular and triangular shapes the scatter plot of Δq_t vs. $\bar{q}_t$ and q_s, respectively. Investigating individual cases (and thus the variability encompassed by the four vertical layers) for shallow clouds, Δq_t for the different layers hardly scales with either q_s or $\bar{q}_t$, with the exception perhaps of the DEEP_cu and DEEP_cb cases and - when comparing to $\bar{q}_t$ - the S11 case. One reason for this is that for the other cases q_s, and less so also $\bar{q}_t$, does not show a large scatter towards the low end. When analysing all six cases for all four layers at the same time, however, some correlation between Δq_t and both q_s and q_t is found, with correlation coefficients r^2 between 0.6 and 0.7. The correlation with q_t (r^2 around 0.7) is somewhat better than the one with q_s (r^2 around 0.6). As such, while far from being perfect, the LES results yield some corroboration for the usefulness of either q_s or $\bar{q}_t$ to determine the distribution width. Consequently, a regression analysis is performed, yielding scaling coefficients between 0.04 and 0.08. These scaling values are much lower than the values used in any of the parameterisations (Tab. 1). A possible reason for the larger values in the parameterisations might be that parameterisations were tuned to yield more realistic cloud cover.

3.3. Parameterised q_t variance

Fig. 3 compares the q_t standard deviation as diagnosed from the LES simulations over the simulation domain to the standard deviation diagnosed from the fitted rectangular and triangular PDFs, respectively (see Appendix for the relationship between variance and Δq_t). The two correlate rather well at r^2 of about 0.8. However, the variance from the rectangular PDF (regression slope of 0.63 and bias of -0.15 g kg^{-1}) and, to a lesser extent

[†]Two other cases are not easy to distinguish from Fig. 1 but are within the limits: In the below-cloud layer for the S11 case, $\bar{q}_s$=9.8 g kg^{-1}, while the maximum q_t=9.7 g kg^{-1}, and in the upper-cloud layer for the DEEP_cu case, $\bar{q}_s$=4.5 g kg^{-1} while maximum q_t=11.4 g kg^{-1}

(regression slope 0.73 and bias of -0.13 g kg^{-1}), from the triangular PDF as well, is underestimating the real variance with biases of -0.13 g^2 kg^{-2} and 0.06 g^2 kg^{-2}, respectively. Overall, correlation coefficient and root-mean-square error suggest the triangular PDF performs slightly better than the rectangular PDF in this metric. The variance can also be diagnosed from Δq_t as parameterised. As expected from the strong scaling of Δq_t with either $\bar{q}_t$ or q_s (Fig. 2), the variance is strongly overestimated by all parameterisations in the cases investigated here. This finding is in contrast to our earlier assessments of the parameterisations (Weber *et al.* 2011; Quaas 2012; Schemann *et al.* 2013). The reason for the small LES-simulated variance or large parameterised one needs to be investigated. One reason could be the relatively small domain used for several of the LES simulations examined. In general, it would be expected that the q_t variance shows some scale-dependence with smaller variance for smaller scales. One of the reasons for this is the occurrence of mesoscale organisation that introduces larger q_t variability at larger scales (Bretherthon *et al.* 2005), and certainly additional variance induced by synoptic variability. Since the RICO case was run on a large domain, we evaluated distribution width Δq_t at domain sizes at 102.4 km, 51.2 km, 25.6 km, 12.8 km and 6.4 km. The results for Δq_t for the smaller domain sizes were not systematically smaller than for the full domain. Rather, they scattered around that value. Perhaps this is the case since RICO is for small cumulus clouds and with a homogeneous surface. This result, however, is also consistent with the results of Quaas (2012) who found that at scales of about 10 km and larger in horizontal domain, the variance is not very scale-dependent. Also in our analysis, while the DEEP_cb case with a domain of 256$\times$256 km^2 tends to show a stronger scaling than average, the DEEP_cu case on the same domain, and the RICO case also on a large (102$\times$102 km^2) domain, do not stand out. Another reason could be the fact that all simulations analysed here apply homogeneous surface conditions and a homogeneous large-scale forcing, while topography, surface inhomogeneities or time-varying large-scale forcings would be expected to introduce stronger q_t variability.

Figure 4. Cloud fraction as simulated by the LES (black), as diagnosed from the LES-simulated PDF but using the integral over the part of the PDF exceeding $\bar{q}_s$ to diagnose cloud fraction (red), using the fitted rectangular PDF (blue), fitted triangular PDF (green), the Smith (1990) parameterisation (magenta), the Sundqvist *et al.* (1989) parameterisation (orange) and the Le Treut and Li (1991) parameterisation (cyan). The bars are ordered from top down in each of the four layers (above cloud - upper cloud - lower cloud - below cloud layers). The panels are for the six cases lower left: S12, upper left: S11, lower middle: S6, upper middle: RICO, lower right: DEEP_cu, upper right: DEEP_cb. The LES-simulated cloud cover in the lower-cloud layer for the RICO case is very small at 0.02%.

3.4. Diagnosed cloud fraction

The fundamental aim of using a diagnosed q_t PDF is to diagnose cloud fraction from it. Cloud fractions diagnosed from the actual, the fitted and parameterised PDFs are shown in comparison to the simulated cloud fraction in Fig. 4. The corresponding statistical comparison of the fits and parameterisations, respectively, to the LES-simulated cloud fractions are given in Table 3. The first test is whether the parameterisations diagnose clouds and clear skies where the LES does so, too. From the actual PDF, even using q_s from the grid-box mean temperature, this is always the case. All other schemes fail at least once; mostly by diagnosing a cloud in the below-cloud layer in the S12 and RICO cases, and by failing to produce clouds in the below-cloud layer in the S11 and S6 cases, as well as (for the fitted PDFs and the Smith (1990) parameterisation) in the two DEEP cases. The parameterised uniform PDFs are rather good in this metric. The correlation between quantified cloud cover and LES-simulated one in all schemes is acceptably good at r^2 between 0.6 and 0.7. The parameterisations show biases of 3 – 8%, RMS of 15 – 19%, and regression slopes in most cases near unity, with the uniform PDF parameterisations yielding some too large values (slope of 0.77). Probably most problematic is the fact that the parameterisations yield too large cloud cover in the partly cloudy situations where in fact the cloud fraction is around or below 10% and the parameterisations yield much larger values. This is especially found for the S12 stratocumulus-over-cumulus and the RICO cumulus cases.

4. Summary and conclusions

Three diagnostic parameterisations for the subgrid-scale variability of the total-water specific humidity, q_t, expressed by rectangular and triangular probability density functions (PDFs), respectively, have been evaluated by the analysis of six different

Table 3. Statistical comparison of the cloud fraction as diagnosed the fits and parameterisations, respectively, in comparison to the LES. r^2 is the correlation coefficient, β the slope of the linear regression, "bias" indicates the mean deviation over the four layers and six cases, "rms", the corresponding root-mean-square error, and "wrong" the percentage of cases where the fit or parameterisation diagnoses a cloud while the LES does not, or the parameterisation diagnoses clear sky where the LES simulates clouds.

	r^2	β	bias	rms	wrong
LES PDF using $\bar{q}_s$	0.72	0.90	0.03	0.15	0%
Fitted rectangular PDF	0.74	1.02	0.06	0.17	25%
Fitted triangular PDF	0.73	1.01	0.05	0.17	17%
Smith (1990)	0.73	1.00	0.04	0.16	29%
Sundqvist *et al.* (1989)	0.59	0.77	0.08	0.19	12%
Le Treut and Li (1991)	0.61	0.77	0.06	0.18	12%

cloud cases simulated using large-eddy simulations (LES). The widths of the PDFs are parameterised as scaling with either the grid-box mean q_t or with the saturation specific humidity, q_s, computed from the grid-box mean temperature. We find that the triangular shape seems close to the LES-simulated q_t PDFs, but that none of the two symmetric PDFs is able to reproduce the often very skewed shapes of the actual PDF.

The width of both rectangular and triangular PDFs indeed relatively well scales with both $\bar{q}_t$ and q_s, with somewhat larger correlation with the former (r^2 of 0.7 rather than 0.6). The scaling coefficient for the LES cases analysed is much lower than suggested by the original parameterisations.

The q_t variance derived from the fitted uniform and triangular PDFs captures the simulated variance relatively well, with a certain underestimation for the uniform shape, and overestimation for the triangular one. That the parameterisations yield a much too large q_t variance is a result contradicting earlier publications evaluating these with satellite data. Reasons could be that the LES simulations examined are partly for rather small domains and driven by homogeneous forcing and boundary conditions.

For the analysed cases, cloud fraction firstly may be diagnosed well from the simulated q_t PDF and q_s derived from the grid-box mean temperature. The fitted, or parameterised, triangular or uniform PDFs wrongly diagnose clouds in cloud-free situations, or no clouds in cloudy situations in 10-30% of the cases. The statistical agreement for the diagnosed and actual cloud cover for all methods is relatively good. However, the sometimes very small actual cloud cover (especially the cumulus cases) is substantially overestimated.

The overall assessment is mixed: q_t variance and cloud cover are statistically relatively well simulated when using a diagnostic q_t PDF of either rectangular or triangular shape. The distribution width is reasonably approximated as scaling with the grid-box mean q_t (better so than when using q_s), but the scaling coefficient is smaller than what the original parameterisations suggest.

Based on the examinations, the suggestion would be that if a simple-shaped PDF is to be used for a cloud parameterisation, the choice of a triangular PDF for which the width scales with the mean q_t as $\Delta q_t = 0.076\ \bar{q}_t$ performs best. However, this is not substantially better than other choices, and limitations of the available LES simulations call for a re-assessment once larger-domain, longer-duration LES simulations with more realistic forcing and surface conditions become available.

Appendix: Variance of the two PDFs

Variance for the rectangular PDF:

$$\begin{aligned}
\sigma^2 &= \int_{-\infty}^{\infty} (q_t - \bar{q}_t)^2 \,\mathrm{PDF}\,(q_t)\ dq_t \\
&= \int_{\bar{q}_t-\Delta q_t}^{\bar{q}_t+\Delta q_t} \frac{1}{2\Delta q_t} (q_t - \bar{q}_t)^2\ dq_t \\
&= \frac{1}{2\Delta q_t} \left[\frac{1}{3}(q_t - \bar{q}_t)^3\right]_{\bar{q}_t-\Delta q_t}^{\bar{q}_t+\Delta q_t} \\
&= \frac{1}{6\Delta q_t} \left[(\bar{q}_t + \Delta q_t - \bar{q}_t)^3 - (\bar{q}_t - \Delta q_t - \bar{q}_t)^3\right] \\
&= \frac{1}{6\Delta q_t} \left[(\Delta q_t)^3 + (\Delta q_t)^3\right] \\
&= \frac{1}{3}(\Delta q_t)^2
\end{aligned}$$

Variance for the triangular PDF:

$$
\begin{aligned}
\sigma^2 &= \int_{-\infty}^{\infty} (q_t - \bar{q}_t)^2 \,\mathrm{PDF}\,(q_t)\; dq_t \\
&= \int_{\bar{q}_t - \Delta q_t}^{\bar{q}_t} (q_t - \bar{q}_t)^2 \,\frac{1}{\Delta q_t}\frac{q_t - (\bar{q}_t - \Delta q_t)}{\Delta q_t}\; dq_t + \\
&\quad \int_{\bar{q}_t}^{\bar{q}_t + \Delta q_t} (q_t - \bar{q}_t)^2 \,\frac{1}{\Delta q_t}\frac{(\bar{q}_t + \Delta q_t) - q_t}{\Delta q_t}\; dq_t \\
&= \frac{1}{(\Delta q_t)^2}\int_{\bar{q}_t - \Delta q_t}^{\bar{q}_t} \left[(q_t - \bar{q}_t)^3 + (q_t - \bar{q}_t)^2\,\Delta q_t\right]\; dq_t + \\
&\quad \frac{1}{(\Delta q_t)^2}\int_{\bar{q}_t}^{\bar{q}_t + \Delta q_t} \left[-(q_t - \bar{q}_t)^3 + (q_t - \bar{q}_t)^2\,\Delta q_t\right]\; dq_t \\
&= \frac{1}{(\Delta q_t)^2}\left(\int_{\bar{q}_t - \Delta q_t}^{\bar{q}_t} (q_t - \bar{q}_t)^3\; dq_t - \int_{\bar{q}_t}^{\bar{q}_t + \Delta q_t} (q_t - \bar{q}_t)^3\; dq_t \right. \\
&\quad \left. + \int_{\bar{q}_t - \Delta q_t}^{\bar{q}_t + \Delta q_t} (q_t - \bar{q}_t)^2\,\Delta q_t\; dq_t\right) \\
&= \frac{1}{(\Delta q_t)^2}\left(\left[\frac{1}{4}(q_t - \bar{q}_t)^4\right]_{\bar{q}_t - \Delta q_t}^{\bar{q}_t} - \left[\frac{1}{4}(q_t - \bar{q}_t)^4\right]_{\bar{q}_t}^{\bar{q}_t + \Delta q_t}\right. \\
&\quad \left. + \left[\frac{1}{3}(q_t - \bar{q}_t)^3\,\Delta q_t\right]_{\bar{q}_t - \Delta q_t}^{\bar{q}_t + \Delta q_t}\right) \\
&= \frac{1}{(\Delta q_t)^2}\left(\frac{1}{4}\left(-(-\Delta q_t)^4 - (\Delta q_t)^4\right)\right. \\
&\quad \left. + \frac{1}{3}\left((\Delta q_t)^3 - (-\Delta q_t)^3\right)\Delta q_t\right) \\
&= \frac{1}{(\Delta q_t)^2}\left(-\frac{1}{2}(\Delta q_t)^4 + \frac{2}{3}(\Delta q_t)^4\right) \\
&= \frac{1}{6}(\Delta q_t)^2
\end{aligned}
$$

Acknowledgements

This work was funded by the Federal Ministry of Education and Research in Germany (BMBF) through the research programme "High Definition Clouds and Precipitation for Climate Prediction - HD(CP)^2" (FKZ: 01LK1210D, 01LK1213B and 01LK1218A), and by the European Research Council in a Starting Grant ("QUAERERE", grant agreement no 306284). Two anonymous reviewers are thanked for their help in improving the study.

References

Blossey PN, Bretherton CS, Zhang M, Cheng A, Endo S, Heus T, Liu Y, Lock AP, de Roode SR, Xu KM. 2013. Marine low cloud sensitivity to an idealized climate change: The CGILS LES intercomparison. *J. Adv. Model. Earth Syst.* **5**: 234–258, doi:10.1002/jame.20025.

Bogenschutz PA, Krueger SK, Khairoutdinov M. 2010. Assumed probability density functions for shallow and deep convection. *J. Adv. Model. Earth Syst.* **2**, doi:10.3894/JAMES.2010.2.10.

Boutle IA, Abel SJ, Hill PG, Morcrette CJ. 2013. Spatial variability of liquid cloud and rain: observations and microphysical effects. *Q. J. R. Meteorol. Soc.* **140**: 583594, doi:10.1002/qj.2140.

Bretherthon CS, Blossey PN, Khairoutdinov M. 2005. An energy-balance analysis of deep convective self-aggregation above uniform SST. *J. Atmos. Sci.* **62**: 4273–4292.

Bryan GH, Wyngaard JC, Fritsch JM. 2003. Resolution requirements for the simulation of deep moist convection. *Mon. Wea. Rev.* **131**: 23942416, doi: 10.1175/1520-0493(2003)131¡2394:RRFTSO¿2.0.CO;2.

Larson VE, Golaz JC, Cotton WR. 2002. Small-scale and mesoscale variability in cloudy boundary layers: Joint probability density functions. *J. Atmos. Sci.* **59**: 3519–3539.

Le Treut H, Li ZX. 1991. Sensitivity of an atmospheric general circulation model to prescribed SST changes: Feedback effects associated with the simulation of cloud optical properties. *Clim. Dyn.* **5**: 175–187.

Naumann AK, Seifert A, Mellado JP. 2013. A refined statistical cloud closure using double-gaussian probability density functions. *Geosci. Model Dev.* **6**: 1641–1657, doi:10.5194/gmd-6-1641-2013.

Perraud E, Couvreux F, Malardel S, Lac C, Masson V, Thouron O. 2011. Evaluation of statistical distributions for the parametrization of subgrid boundary-layer clouds. *Boundary-Layer Meteorol.* **140**: 263–294, doi: 10.1007/s10546-011-9607-3.

Petch JC, Brown AR, Gray MEB. 2002. The impact of horizontal resolution on the simulations of convective development over land. *Q. J. R. Meteorol. Soc.* **128**: 20312044, doi:10.1256/003590002320603511.

Quaas J. 2012. Evaluating the "critical relative humidity" as a measure of subgrid-scale variability of humidity in general circulation model cloud cover parameterizations using satellite data. *J. Geophys. Res.* **117**: D09 208, doi:10.1029/2012JD017495.

Roeckner E, Bäuml G, Bonaventura L, Brokopf R, Esch M, Giorgetta M, Hagemann S, Kirchner I, Kornblueh L, Manzini E, Rhodin A, Schlese U, Schulzweida U, Tompkins A. 2003. The atmospheric general circulation model ECHAM5: Part I: Model description. In: *Report*, vol. 349. Max Planck Institute for Meteorology, p. 127pp.

Schemann V, Stevens B, Grützun V, Quaas J. 2013. Scale dependency of total water variance, and its implication for cloud parameterizations. *J. Atmos. Sci.* **70**: 3615–3630, doi:10.1175/JAS-D-13-09.1.

Schlemmer L, Hohenegger C. 2014. The formation of wider and deeper clouds as a result of cold-pool dynamics. *J. Atmos. Sci.* **71**: 2842–2858, doi: 10.1175/JAS-D-13-0170.1.

Seifert A, Heus T. 2013. Large-eddy simulation of organized precipitating trade wind cumulus clouds. *Atmos. Chem. Phys.* **13**: 5631–5645, doi: 10.5194/acp-13-5631-2013.

Smith RN. 1990. A scheme for predicting layer clouds and their water content in a general circulation model. *Q. J. R. Meteorol. Soc.* **116**: 435–460, doi: 10.1002/qj.49711649210.

Stevens B, Giorgetta M, Esch M, Mauritsen T, Crueger T, Rast S, Salzmann M, Schmidt H, Bader J, Block K, Brokopf R, Fast I, Kinne S, Kornblueh L, Lohmann U, Pincus R, Reichler R, Roeckner E. 2013. Atmospheric component of the MPI-M Earth System Model: ECHAM6. *J. Adv. Model. Earth Syst.* **5**: 146–172, doi:10.1002/jame.20015.

Stevens B, Moeng CH, Ackerman AS, Bretherton CS, Chlond A, de Roode S, Edwards J, Golaz JC, Jiang H, Khairoutdinov M, Kirkpatrick MP, Lewellen DC, Lock A, Müller F, Stevens DE, Whelan E, Zhu P. 2005. Evaluation of large-eddy simulations via observations of nocturnal marine stratocumulus. *Mon. Wea. Rev.* **133**: 1443–1462, doi:10.1175/MWR2930.1.

Sundqvist H, Berge E, Kristjánsson JE. 1989. Condensation and cloud parameterization studies with a mesoscale numerical weather prediction model. *Mon. Wea. Rev.* **117**: 1641–1657.

Tompkins A. 2002. A prognostic parameterization for the subgrid-scale variability of water vapor and clouds in large-scale model and its use to diagnose cloud cover. *J. Atmos. Sci.* **59**: 1917–1942.

VanZanten MC, Stevens B, Nuijens L, Siebesma A, Ackerman A, Burnet F, Cheng A, Couvreux F, Jiang H, Khairoutdinov M, Kogan Y, Lewellen D, Mechem D, Nakamura K, Noda A, Shipway B, Slawinska J, Wang S, Wyszogrodzki A. 2011. Controls on precipitation and cloudiness in simulations of trade-wind cumulus as observed during RICO. *J. Adv. Model. Earth Syst.* **3**: M06 001, doi:10.1029/2011MS000056.

Watanabe M, Emori S, Satoh M, Miura H. 2009. A PDF-based hybrid prognostic cloud scheme for general circulation models. *Clim. Dyn.* **33**: 795–816, doi:10.1007/s00382-008-0489-0.

Weber T, Quaas J, Räisänen P. 2011. Evaluation of the subgrid-scale variability scheme for water vapor and cloud condensate in the ECHAM5 model using satellite data. *Q. J. R. Meteorol. Soc.* **137**: 2079–2091, doi:10.1002/qj.887.

Zhang M, Bretherton CS, Blossey PN, Austin PH, Bacmeister JT, Bony S, Brient F, Cheedela SK, Cheng A, Del Genio AD, De Roode SR, Endo S, Franklin CN, Golaz JC, Hannay C, Heus T, Isotta FA, Dufresne JL, Kang IS, Kawai H, Larson MKVE, Liu Y, Lock AP, Lohmann U, Khairoutdinov MF, Molod AM, Neggers RAJ, Rasch P, Sandu I, Senkbeil R, Siebesma AP, Siegenthaler-Le Drian C, Stevens B, Suarez MJ, Xu KM, von Salzen K, Webb MJ, Wolf A, Zhao M. 2013. CGILS: Results from the first phase of an international project to understand the physical mechanisms of low cloud feedbacks in single column models. *J. Adv. Model. Earth Syst.* **5**: 826–842, doi:10.1002/2013MS000246.

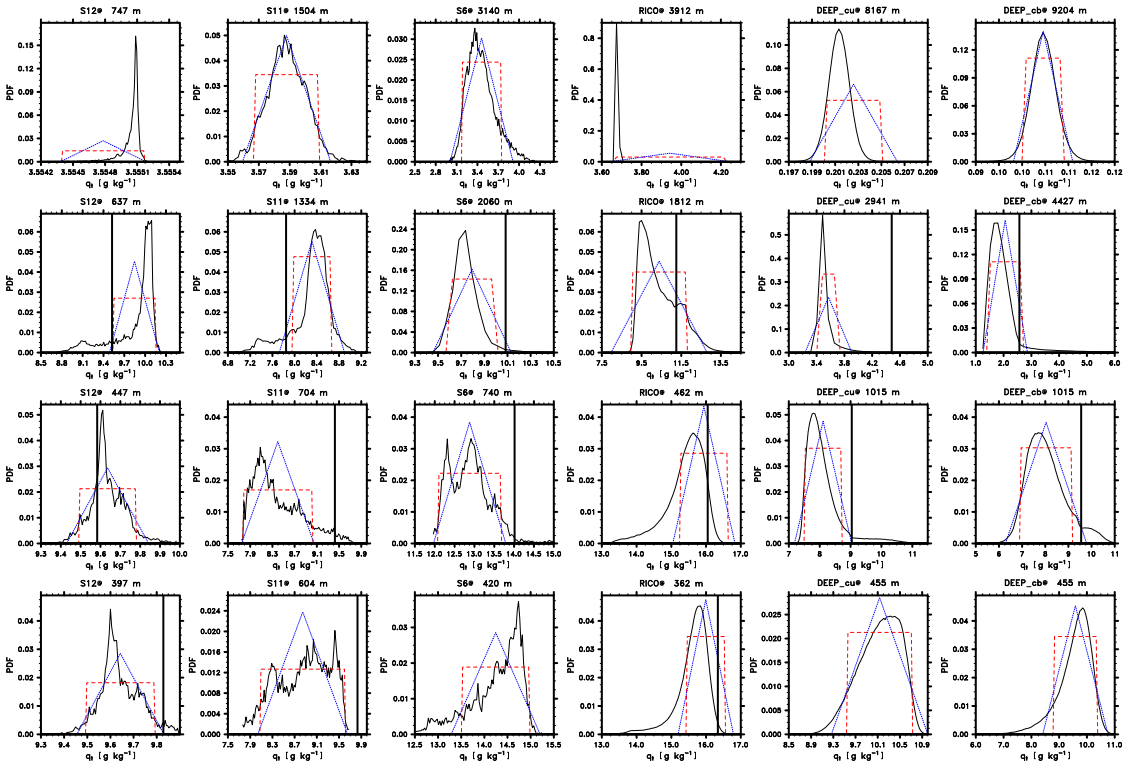

Figure 1. PDFs of q_t as simulated by the LES (black plain), fitted rectangular (red, dashed) and triangular (blue, dotted) PDFs. The vertical black line indicates q_s diagnosed from the domain-mean temperature. Columns from left to right are the S11, S12, S6, RICO, DEEP_cu and DEEP_cb cases. Rows are for each case selected layers, from top to bottom: above cloud top, in upper part of cloud, in lower part of the cloud, below cloud base. For each case, a time-step representative of the developed, where applicable: equilibrium, cloud regime is selected.

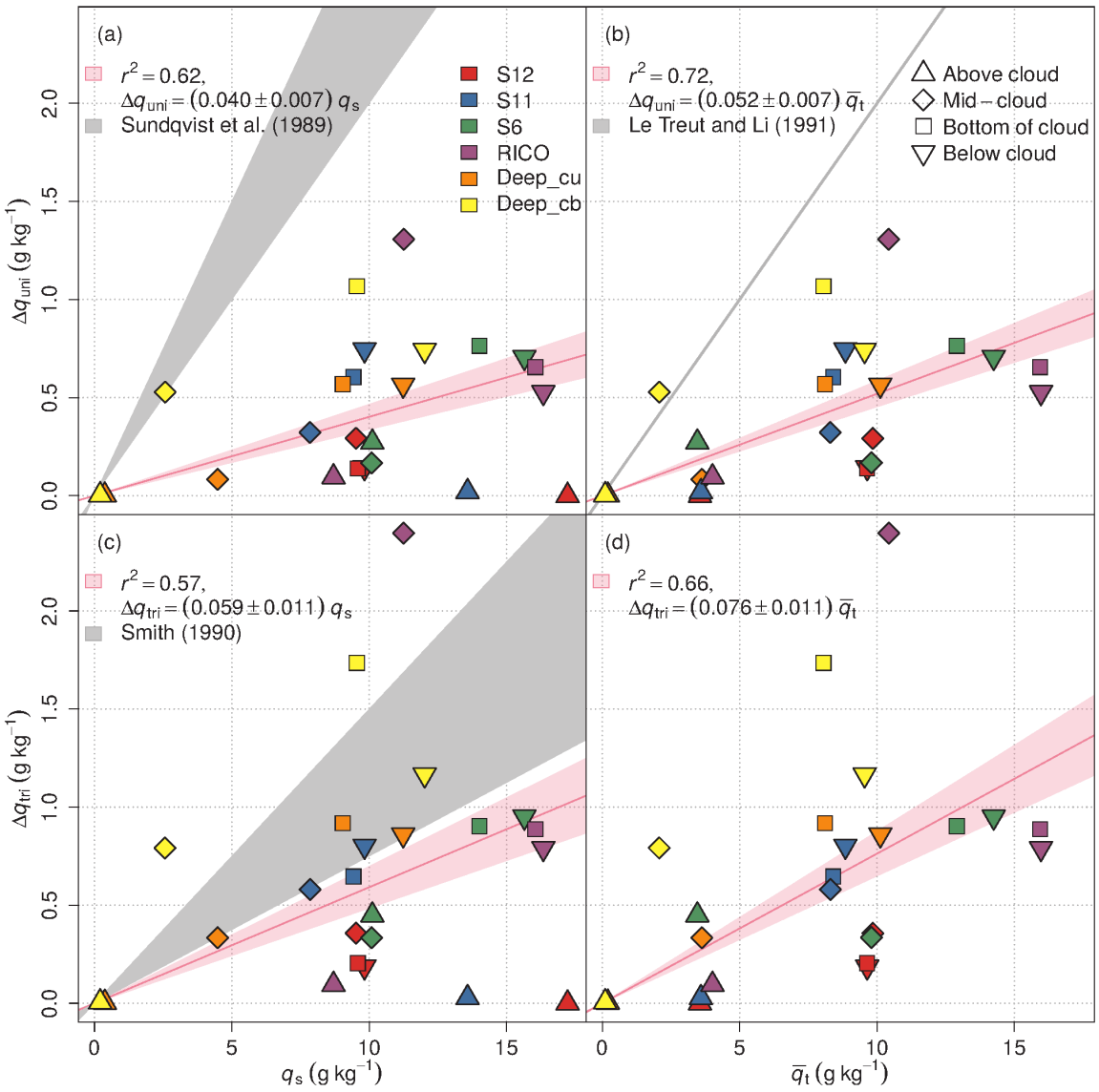

Figure 2. Scatterplot of distribution width for (a,c) rectangular and (b,d) triangular shapes as a function of (a,b) q_t and (c,d) q_s for the cases shown in Fig. 1. Red: S12, blue: S11, green: S6, purple: RICO, orange: DEEP_cu, yellow: DEEP_cb. Triangles up: above-cloud level, diamonds: upper cloud level, squares: lower cloud level, triangles down: below-cloud level. The red line indicates the regression fit forced through zero, and the pink shading $\pm$ one standard deviation of the fit. The grey-shaded area in (a) encompasses the near-surface and free-troposphere values of the Sundqvist *et al.* (1989) parameterisation, the grey line in (b) is the Le Treut and Li (1991) parameterisation, and the grey-shaded area in (c), the range as parameterised by Smith (1990).

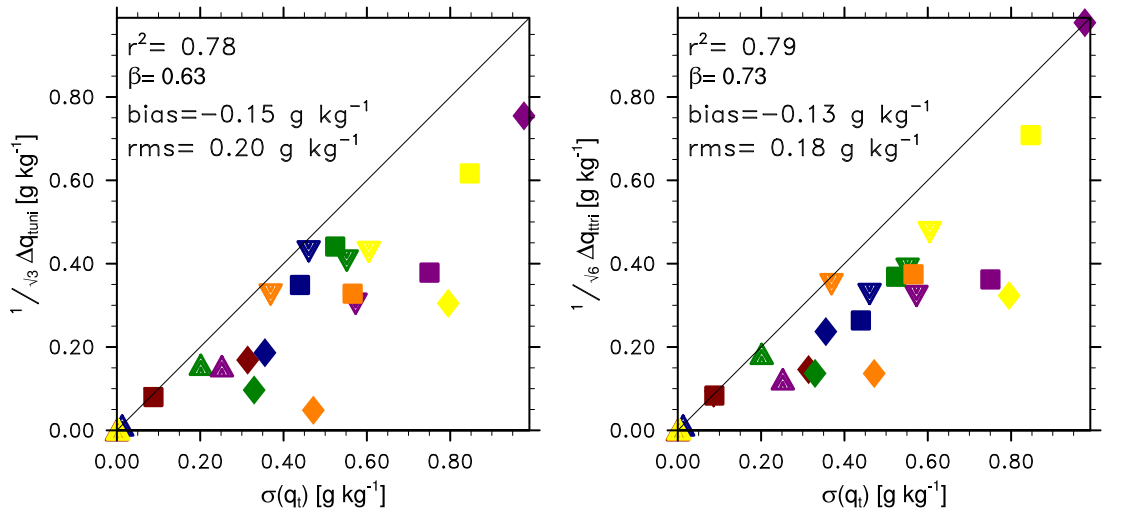

Figure 3. Scatterplot of the standard deviation of q_t as computed from the LES data vs. (left) the standard deviation as computed by the fitted uniform and (right) the fitted triangular PDF. Cases are by colour and layers by symbol as in Fig. 2. Statistics are given in the upper left of each panel, i.e., the correlation coefficient r^2, the slope of the linear regression line, β, the mean bias standard deviation of the fit minus of the LES data, and corresponding root-mean-square deviation.

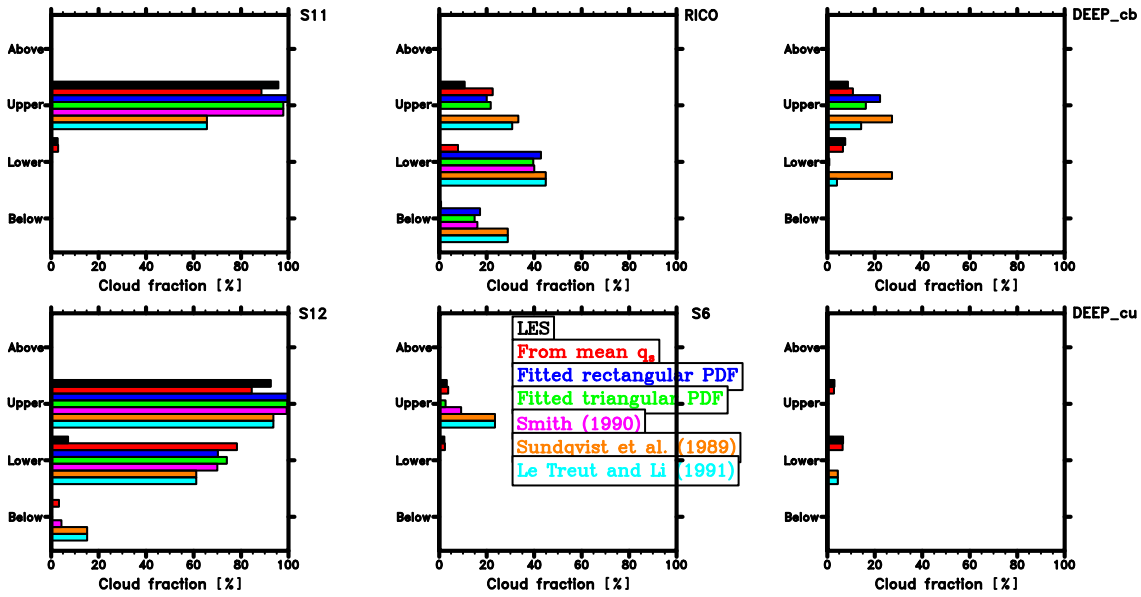

Figure 4. Cloud fraction as simulated by the LES (black), as diagnosed from the LES-simulated PDF but using the integral over the part of the PDF exceeding $\bar{q}_s$ to diagnose cloud fraction (red), using the fitted rectangular PDF (blue), fitted triangular PDF (green), the Smith (1990) parameterisation (magenta), the Sundqvist *et al.* (1989) parameterisation (orange) and the Le Treut and Li (1991) parameterisation (cyan). The bars are ordered from top down in each of the four layers (above cloud - upper cloud - lower cloud - below cloud layers). The panels are for the six cases lower left: S12, upper left: S11, lower middle: S6, upper middle: RICO, lower right: DEEP_cu, upper right: DEEP_cb. The LES-simulated cloud cover in the lower-cloud layer for the RICO case is very small at 0.02%.